analytical chemistry

pubs.acs.org/ac

Letter

A Self-Immolative Fluorescent Probe for Selective Detection of SARS-CoV-2 Main Protease

Ming Xu, Jiajing Zhou, Yong Cheng, Zhicheng Jin, Alex E. Clark, Tengyu He, Wonjun Yim, Yi Li, Yu-Ci Chang, Zhuohong Wu, Pavla Fajtová, Anthony J. O'Donoghue, Aaron F. Carlin, Michael D. Todd, and Jesse V. Jokerst*

Cite This: *Anal. Chem.* 2022, 94, 11728−11733

Read Online

ACCESS | Metrics & More | Article Recommendations | Supporting Information

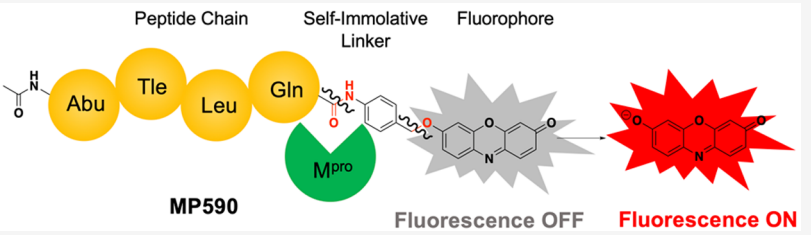

ABSTRACT: Existing tools to detect and visualize severe acute respiratory syndrome coronavirus 2 (SARS-CoV-2) suffer from low selectivity, poor cell permeability, and high cytotoxicity. Here we report a novel self-immolative fluorescent probe (MP590) for the highly selective and sensitive detection of the SARS-CoV-2 main protease (M^{pro}). This fluorescent probe was prepared by connecting a M^{pro}-cleavable peptide (*N*-acetyl-Abu-Tle-Leu-Gln) with a fluorophore (*i.e.*, resorufin) via a self-immolative aromatic linker. Fluorescent titration results show that MP590 can detect M^{pro} with a limit of detection (LoD) of 35 nM and is selective over interferents such as hemoglobin, bovine serum albumin (BSA), thrombin, amylase, SARS-CoV-2 papain-like protease (PL^{pro}), and trypsin. The cell imaging data indicate that this probe can report M^{pro} in HEK 293T cells transfected with a M^{pro} expression plasmid as well as in TMPRSS2-VeroE6 cells infected with SARS-CoV-2. Our results suggest that MP590 can both measure and monitor M^{pro} activity and quantitatively evaluate M^{pro} inhibition in infected cells, making it an important tool for diagnostic and therapeutic research on SARS-CoV-2.

The coronavirus disease 2019 (COVID-19) pandemic[1] is caused by severe acute respiratory syndrome coronavirus 2 (SARS-CoV-2), which is a single-stranded RNA coronavirus that can cause severe respiratory disease.[1] Symptoms of COVID-19 include fever, chills, headache, sore throat, cough, and fatigue, and this virus is much more infectious than other common diseases.[2] Numerous methods have been developed to detect and monitor SARS-CoV-2;[3−7] however, these approaches can seldom be used to accurately visualize virus activity in infected cells. One reliable way to visualize SARS-CoV-2 in infected cells is to look into the roles of the critical proteases in the viral lifecycle, for example, the SARS-CoV-2 papain-like protease (PL^{pro}) and the main protease (M^{pro} or $3CL^{pro}$).[8,9] M^{pro} is a key protease of SARS-CoV-2 that controls viral reproduction[10,11] by producing nonstructural proteins.[10,12,13] Unlike other proteases in SARS-CoV-2, M^{pro} is so unique that nearly no human protease shares a similar structure or function, which makes it an idea biomarker for visualizing SARS-CoV-2 and its activity.[8] The selective and sensitive detection of M^{pro} in cells could help monitor and stratify viral replication as well as develop highly effective drugs for SARS-CoV-2 therapy.

Recently, many approaches have been developed for the detection of M^{pro},[14−18] among which electrochemical sensors, colorimetric sensors, and genetically encoded biosensors have been the most popular. In 2022, the Liu group developed a versatile electrochemical sensor that took advantage of the peptide-triggered assembly of gold nanoparticles to introduce an electrochemical signal for M^{pro} detection.[14] Despite that fact that the levels of detection (LoDs) of the electrochemical sensors can be as low as 0.1 pM, these sensors rarely detect M^{pro} in real cell samples due to their low electrochemical stability in cells.[14] Another useful approach for detecting M^{pro} is the colorimetric sensor.[14,17,19,20] One representative gold nanoparticle-based colorimetric protease assay was reported by Willis and coauthors to detect the exogenously expressed M^{pro} in HEK 293T cells.[19] Meanwhile, based on the versatility of

Received: June 3, 2022
Accepted: August 10, 2022
Published: August 16, 2022

https://doi.org/10.1021/acs.analchem.2c02381
Anal. Chem. 2022, 94, 11728−11733

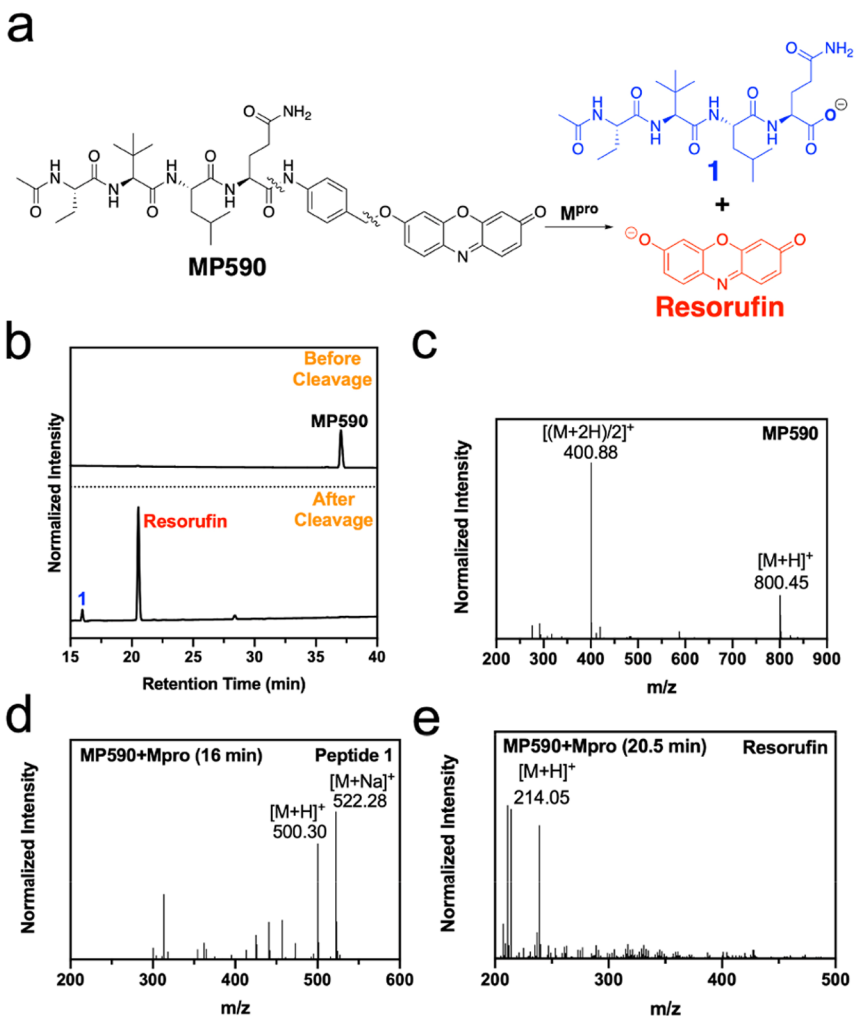

Figure 1. Detection mechanism of MP590. (a) The proposed cleavage mechanism of MP590 upon treatment with M^{pro}. (b) HPLC data of MP590 before (top) and after (bottom) incubation with M^{pro} (100 nM) in Tris buffer (20 mM Tris and 150 mM NaCl, pH 7.4) at 37 °C for 2.5 h. (c) ESI-MS positive-mode data of pure MP590. (d) ESI-MS positive-mode data of the MP590 cleavage product at ∼16 min. (e) ESI-MS positive-mode data of the MP590 cleavage product at ∼20.5 min.

nanomaterials,[21−26] we developed sensitive colorimetric sensors for the detection of M^{pro}.[17,20,27] However, these colorimetric sensors cannot be used to accurately visualize M^{pro} activity in infected cells. As another approach, genetically encoded biosensors have generated several excellent sensors for M^{pro}.[28,29] Although these genetically encoded biosensors provide the selective and noninvasive detection of M^{pro}, they can only be used in gene-edited cells.

Fluorescence as a nondestructive energy form can be used to achieve the sensitive, measurable, and contrastive detection of all kinds of biological molecules.[30−34] Recently, many fluorescent probes have been developed to detect the SARS-CoV-2 M^{pro} (Table S1). One representative example is a flipped split green fluorescent protein (FlipGFP) reporter, which exhibited a 100-fold fluorescence enhancement upon the introduction of transfected M^{pro}.[35] However, this reporter has to be used in plasmid-transfected cells, and it takes at least 24 h to finish the incubation. A series of fluorogenic-based substrates (HyCoSuL) were developed to detect M^{pro} in 2021.[18] These substrates can be used to recognize M^{pro} in cells, but they are limited to use with some specific dyes (*e.g.*, 7-amino-4-carbamoylmethylcoumarin) that can directly bind a M^{pro}-cleavable peptide. There are two other popular fluorescent probes for M^{pro}: a cyclodextrin-based protease-activatable moiety[36] and a Förster resonance energy transfer (FRET) dual-color probe.[16] Both these two probes are versatile probes with excellent performances; however, their preparations involve too many complicated synthesis steps (a 12-step synthesis for the cyclodextrin-based protease-activatable probe and a 6-step synthesis for the FRET design), limiting their applications.

In this work, we report a self-immolative fluorescent probe (MP590) for the detection and imaging of the SARS-CoV-2 main protease M^{pro}. This fluorescent probe (MP590) (Figure 1) consists of three parts: a M^{pro}-cleavable peptide chain (*N*-acetyl-Abu-Tle-Leu-Gln),[18] a fluorophore (resorufin), and a self-immolative aromatic linker named 4-aminobenzyl alcohol (PABA). The probe itself was prepared by connecting the resorufin group (fluorophore) with the peptide chain (*N*-acetyl-Abu-Tle-Leu-Gln) via the 4-aminobenzyl alcohol linker, which exhibited relatively weak fluorescence. The amide bond between the peptide and the 4-aminobenzyl alcohol linker can be cleaved in the presence of M^{pro}. Subsequently, a free amine group will be released on the linker and will push the lone-pair

https://doi.org/10.1021/acs.analchem.2c02381
Anal. Chem. 2022, 94, 11728−11733

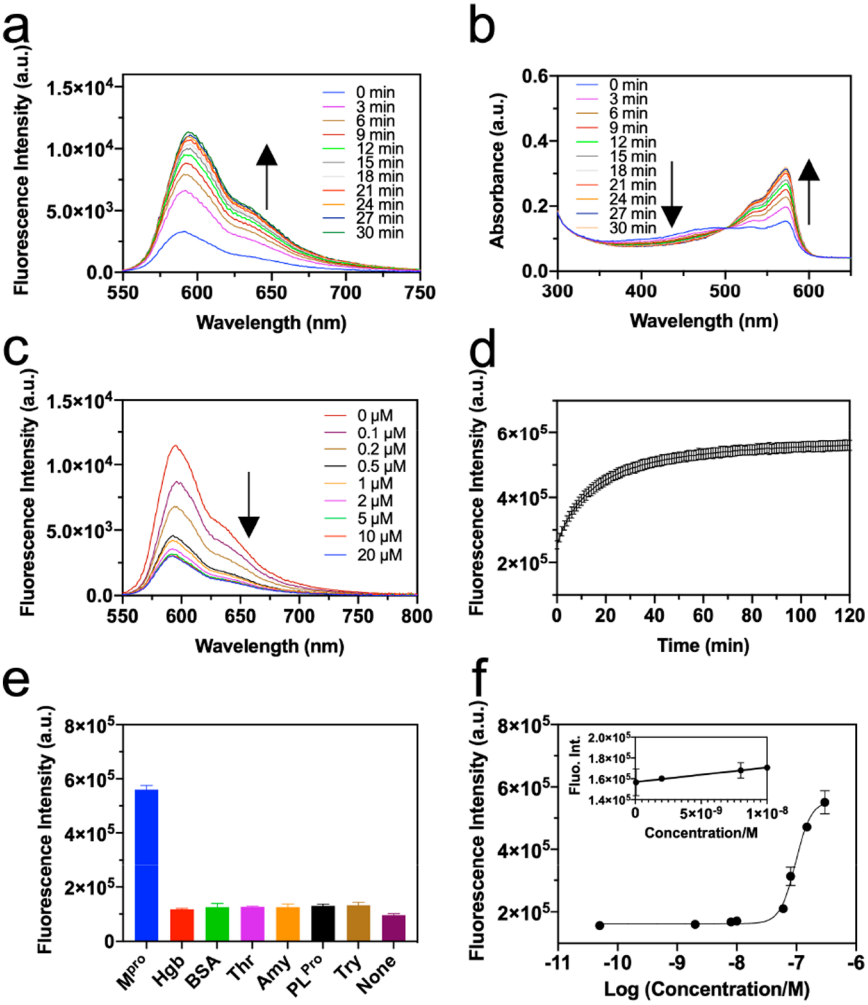

Figure 2. Fluorescence and UV−vis data of MP590. (a) Fluorescence spectra and (b) UV−vis absorbance spectra of MP590 (50 μM) incubated with M^{pro} (150 nM) at 37 °C. (c) Fluorescence spectra of MP590 incubated with M^{pro} (150 nM) and the M^{pro} inhibitor (GC376) with a concentration range from 0 to 20 μM at 37 °C. (d) Fluorescence kinetics of MP590 incubated with M^{pro} (150 nM) at 37 °C. (e) Selectivity tests of MP590 with different analytes including hemoglobin (Hgb), bovine serum albumin (BSA), thrombin (Thr), amylase (Amy), papain-like protease (PL^{pro}), and trypsin (Try). (f) Fluorescent LoD experiments for MP590 at 30 min (the insert shows the linear fit of the MP590 concentration versus the fluorescence intensity). All probes were dissolved in Tris buffer (20 mM Tris; 150 mM NaCl, pH 7.4; and 1% DMSO). All data were based on triplicate titrations (excitation at 514 nm). The error bars represent the standard deviation.

electrons toward the resorufin group; afterward, this resorufin dye acts as a leaving group and disassembles. Thus, the cleavage of the fluorescence reporter substrate by M^{pro} will yield a fluorescence signal that can be used to detect and image M^{pro}.

Probe MP590 was synthesized as shown in Scheme S1.[36] To confirm that MP590 could be cleaved by M^{pro} (Figure 1a), we incubated MP590 (5 μM) in Tris buffer (20 mM Tris and 150 mM NaCl, pH 7.4) with M^{pro} (100 nM) at 37 °C for 2.5 h and checked the final products and the pure probe (MP590) using high-performance liquid chromatography (HPLC) and electrospray ionization mass spectrometry (ESI-MS). Results show that pure MP590 was eluted from the HPLC column at about 37 min (Figure 1b); its mass was confirmed by ESI-MS (Figure 1c). The incubation product was purified using the same HPLC protocol, and its HPLC data show no peak at 37 min (Figure 1b). Instead, there are two main peaks at about 16 and 20.5 min, which were confirmed by ESI-MS to be compound **1** and resorufin (Figure 1d and e). These data validate that MP590 can be cleaved by M^{pro}.

We evaluated the stability of this probe by preparing MP590 in different buffers using fluorescence (Figure S1). The results show that this probe is stable in common buffers, including Tris buffer, Dulbecco's phosphate buffered saline (DPBS), Dulbecco's modified Eagle medium (DMEM), and real cell culture medium. Next, we prepared MP590 in Tris buffer (20 mM Tris and 150 mM NaCl, pH 7.4) and incubated it with M^{pro}. After the addition of M^{pro} (150 nM) to MP590 (50 μM), an increase in fluorescence at 590 nm (Figure 2a) and an enhancement in absorbance at 570 nm (Figure 2b) were observed within 30 min. The isosbestic point at about 500 nm in the UV−vis spectrum indicated that the introduction of M^{pro} could result in the formation of new product in the probe solution, which validated the proposed cleavage mechanism.

To confirm that the fluorescence signal enhancement came from the M^{pro} cleavage reaction, we next designed an inhibition assay for M^{pro} (Figure 2c). Specifically, MP590 (50 μM) was incubated with both M^{pro} (150 nM) and a commercial M^{pro} inhibitor GC376 (0−20 μM) and scanned after 30 min of incubation at 37 °C. The data show that the fluorescence

https://doi.org/10.1021/acs.analchem.2c02381
Anal. Chem. 2022, 94, 11728−11733

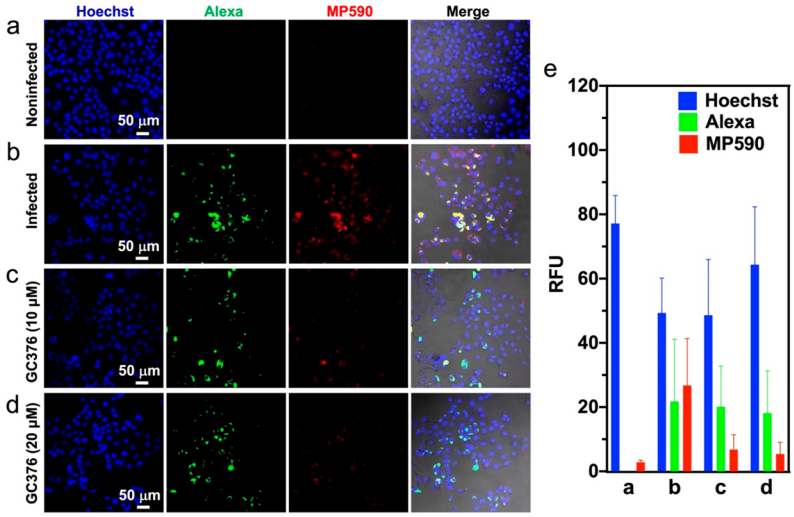

Figure 3. Visualization of M^{pro} and M^{pro} inhibition activity by MP590 in SARS-CoV-2-infected TMPRSS2-VeroE6 cells. The TMPRSS2-VeroE6 cells were treated as follows: (a) TMPRSS2-VeroE6 cells with no infection treatment, (b) TMPRSS2-VeroE6 cells were infected with SARS-CoV-2, (c) SARS-CoV-2-infected TMPRSS2-VeroE6 cells were treated with 10 μM of a commercial M^{pro} inhibitor (GC376), and (d) SARS-CoV-2-infected TMPRSS2-VeroE6 cells were treated with 20 μM GC376. Panel a shows that uninfected TMPRSS2-VeroE6 cells present very dim fluorescent signals. Panel b shows that infected TMPRSS2-VeroE6 cells exhibit an obvious increase in fluorescence in both the M^{pro} antibody (alexa) and MP590 channels. Panel c shows the clear decrease of fluorescence emissions in both the M^{pro} antibody (alexa) and MP590 channels after the infected TMPRSS2-VeroE6 cells were incubated with 10 μM GC376. Panel d shows further fluorescence signal decreases in both the M^{pro} antibody (alexa) and MP590 channels after the GC376 concentration was increased from 10 to 20 μM. (e) Mean fluorescence intensity and standard deviation (error bars) of CLSM images (12 fields of view) from panels a–d. All cell lines were treated with MP590 (3 μM) and SARS-CoV-2 M^{pro} primary and secondary (alexa) antibodies.

signal decreases as the concentration of the inhibitor increases, confirming that M^{pro} cleaved the probe MP590 and activated the fluorescence. The progress curve shows that it takes about 30 min for MP590 to be cleaved by M^{pro} (Figure 2d).

We also tested the probe with some common protein interferents under the same conditions. Hemoglobin, BSA, thrombin, amylase, PL^{pro}, and trypsin generated negligible changes in fluorescence when titrated with MP590 (Figure S2). In contrast, M^{pro} (150 nM) could increase the fluorescence of the probe sixfold (Figure 2e). The LoD of MP590 for M^{pro} at 30 min is 35 nM (see the Supporting Information for the full calculation) (Figures 2f and S3).[37]

We next evaluated the cytotoxicity and background fluorescence of MP590 in cells. We first checked the cytotoxicity of the probe design by incubating the HEK 293T cells with different concentrations of MP590 (1, 5, 10, 20, and 40 μM). The results show that the cell viability was approximately 90% in the presence of up to 20 μM MP590 (Figure S9b). Meanwhile, we incubated the HEK 293T cells with MP590 cleavage products, including peptide **1** and resorufin, and found that both two products showed no obvious toxicity to cells at concentrations below 20 μM (cell viabilities were about 90%) (Figure S9b). We next evaluated the background fluorescence of the probe by incubating HEK 293T cells with different concentrations of MP590 (1, 3, and 5 μM) and checking them using confocal laser scanning microscopy (CLSM) (Figure S4). We selected 3 μM as the probe incubation concentration because this concentration offered good contrast, low background, and no toxicity.

To further evaluate the performance of MP590, we used CLSM to measure the level of M^{pro} in plasmid-transfected HEK 293T cells (Figure S5). We transfected HEK 293T cells with plasmids expressing M^{pro}, a M^{pro}-cleavable self-assembling FlipGFP, or a negative control influenza protease (PR8) unable to cleave MP590 or FlipGFP, as reported by the Heaton Group.[35] FlipGFP is a M^{pro} reporter protein that is prepared by connecting two independent GFPs (β10 and β11) in parallel with a M^{pro}-cleavable linker. When M^{pro} cleaves the linker of FlipGFP, the two GFP moieties are antiparallel (fit in GFPs β1–9), which turns on the fluorescence signal of the system (Figure S5e); otherwise, the signal is off.[35] Thus, FlipGFP confirms the successful transfection of M^{pro} plasmids but has limited utility in endogenously expressed M^{pro}.

We first incubated HEK 293T cells with MP590 and Hoechst 33258 (cell-permeable nucleic acid stain) and imaged them using CLSM. MP590 (emission at 590 nm) alone exhibited minimal background fluorescence after 30 min (Figure S5a). HEK 293T cells were then transfected with FlipGFP and incubated with MP590. Both the GFP and MP590 channels showed weak fluorescence, since there was no M^{pro} expressed in these cells (Figure S5b). We also incubated HEK 293T cells expressing both PR8 (negative control protein) and FlipGFP with MP590 for 30 min, resulting in dim fluorescence signals in both the GFP and MP590 channels (Figure S5c). As we expected, PR8 could not cleave MP590, and FlipGFP was not activated. In contrast, after incubating M^{pro}-expressing HEK 293T cells with MP590, there was a clear increase in colocalized fluorescence in the GFP and MP590 channels, thus confirming that MP590 selectively stained M^{pro}-expressing HEK 293T cells (Figure S 5d,f).

We next studied the capacity of MP590 to visualize M^{pro} and M^{pro} inhibition in TMPRSS2-expressing VeroE6 (TMPRSS2-VeroE6) cells infected with authentic SARS-CoV-2 (Figure 3). TMPRSS2-VeroE6 cells incubated with up to 10 μM MP590 for 30 min showed minimal background fluorescence (Figures 3a and S6). Next, we infected TMPRSS2-VeroE6 cells with SARS-CoV-2 (USA-WA1/2020, BEI NR-52281) at a multiplicity of infection (MOI) of 0.5 for 24 h, treated the infected

https://doi.org/10.1021/acs.analchem.2c02381
Anal. Chem. 2022, 94, 11728–11733

cells with MP590 for 30 min, fixed the treated cells with 4% formaldehyde, and stained the fixed cells with Hoechst 33258 and a M^{pro} antibody (anti-SARS-CoV-2 M^{pro} primary antibody and AlexaFluor 488-labeled secondary antibody). The CLSM data show that MP590 and M^{pro} antibody stains colocalize in SARS-CoV-2-infected TMPRSS2-VeroE6 cells (Figures 3b, S7, and S9a). This indicates that MP590 identifies SARS-CoV-2-infected TMPRSS2-VeroE6 cells. We next infected TMPRSS2-VeroE6 cells with SARS-CoV-2 for 18 h and then treated them with both MP590 and the commercial M^{pro} protease inhibitor (GC376) for 30 min. Cells were formaldehyde-fixed and stained with M^{pro} antibodies and Hoechst 33258. Treatment with GC376 decreased the fluorescence intensity in the MP590 channel without altering M^{pro} staining in SARS-CoV-2-infected cells (Figures 3c, d, and e and S8). These results collectively demonstrate that the probe can be used to monitor the enzymatic activity of M^{pro} in infected cells, which opens up new avenues to explore the diagnosis and treatment of COVID-19.

In conclusion, we reported a self-immolative fluorescent probe (MP590) for the selective detection of SARS-CoV-2 M^{pro}. Fluorescent data show that M^{pro} can be used to cleave MP590 and turn on the fluorescent signal of the system. This detection mechanism was confirmed by HPLC and mass spectroscopy. Meanwhile, MP590 shows very high selectivity compared to other common protein interferents such as hemoglobin, BSA, thrombin, amylase, PL^{pro}, and trypsin. The cell imaging data indicate that the fluorescent probe MP590 can visualize SARS-CoV-2 M^{pro} in both plasmid-transfected HEK 293T cells and SARS-CoV-2-infected TMPRSS2-VeroE6 cells. In the plasmid-transfected HEK 293T cells, we successfully verified the imaging of M^{pro} with MP590 using the M^{pro} reporter protein FlipGFP and the control protein PR8. In the SARS-CoV-2-infected TMPRSS2-VeroE6 cells, we demonstrated that activated MP590 could be used to detect M^{pro} in infected cells, which was validated by the reduction in the fluorescence signal in the presence of GC376. The results indicate that MP590 can report the strength of SARS-CoV-2 M^{pro} inhibition in infected cells when treated with different concentrations of GC376. We envision that MP590 could provide a very useful and effective tool to visualize M^{pro} activity as well as M^{pro} inhibition in SARS-CoV-2-infected cells.

■ ASSOCIATED CONTENT

Supporting Information

The Supporting Information is available free of charge at https://pubs.acs.org/doi/10.1021/acs.analchem.2c02381.

Materials, instruments, methods, synthetic procedures, HPLC data, ESI-MS data, fluorescence spectra, LoD measurements, CLSM imaging data, and the cytotoxicity assay (PDF)

■ AUTHOR INFORMATION

Corresponding Author

Jesse V. Jokerst − *Department of NanoEngineering, University of California, San Diego, La Jolla, California 92093, United States; Materials Science and Engineering Program and Department of Radiology, University of California, San Diego, La Jolla, California 92093, United States;* orcid.org/0000-0003-2829-6408; Email: jjokerst@eng.ucsd.edu

Authors

Ming Xu − *Department of NanoEngineering, University of California, San Diego, La Jolla, California 92093, United States;* orcid.org/0000-0002-6998-8462

Jiajing Zhou − *Department of NanoEngineering, University of California, San Diego, La Jolla, California 92093, United States;* orcid.org/0000-0001-5203-4737

Yong Cheng − *Department of NanoEngineering, University of California, San Diego, La Jolla, California 92093, United States*

Zhicheng Jin − *Department of NanoEngineering, University of California, San Diego, La Jolla, California 92093, United States;* orcid.org/0000-0001-6072-7533

Alex E. Clark − *Department of Pathology and Medicine, University of California, San Diego, La Jolla, California 92093, United States*

Tengyu He − *Materials Science and Engineering Program, University of California, San Diego, La Jolla, California 92093, United States;* orcid.org/0000-0002-6767-4849

Wonjun Yim − *Materials Science and Engineering Program, University of California, San Diego, La Jolla, California 92093, United States;* orcid.org/0000-0002-0242-7898

Yi Li − *Department of NanoEngineering, University of California, San Diego, La Jolla, California 92093, United States*

Yu-Ci Chang − *Materials Science and Engineering Program, University of California, San Diego, La Jolla, California 92093, United States;* orcid.org/0000-0001-6997-9884

Zhuohong Wu − *Department of NanoEngineering, University of California, San Diego, La Jolla, California 92093, United States*

Pavla Fajtová − *Skaggs School of Pharmacy and Pharmaceutical Sciences, University of California, San Diego, La Jolla, California 92093, United States*

Anthony J. O'Donoghue − *Skaggs School of Pharmacy and Pharmaceutical Sciences, University of California, San Diego, La Jolla, California 92093, United States;* orcid.org/0000-0001-5695-0409

Aaron F. Carlin − *Department of Pathology and Medicine, University of California, San Diego, La Jolla, California 92093, United States;* orcid.org/0000-0002-1669-8066

Michael D. Todd − *Department of Structural Engineering, University of California, San Diego, La Jolla, California 92093, United States;* orcid.org/0000-0002-4492-5887

Complete contact information is available at: https://pubs.acs.org/10.1021/acs.analchem.2c02381

Notes

The authors declare no competing financial interest.

■ ACKNOWLEDGMENTS

The authors acknowledge the UC Office of the President for the internal grant (R00RG2515) and the National Institutes of Health (R21 AI157957, R01 DE031114, and R21 AG065776-S1) for financial support. This research project was also supported by the National Science Foundation (1845683) and NINDS P30NS047101 to the UCSD microscopy core. A.F.C. acknowledges the financial support from NIH grant (K08AI130381) and the Career Award for Medical Scientists from the Burroughs Wellcome Fund. The authors graciously thank Prof. Rolf Hilgenfeld (Institute of Biochemistry at University of Lübeck), Prof. Liangfang Zhang (Department of

Nanoengineering at University of California San Diego), and Prof. Nicholas S. Heaton (Department of Molecular Genetics and Microbiology at Duke University School of Medicine) for providing HEK 293T cells and plasmids. We obtained the following reagent through BEI Resources, NIAID, NIH: SARS-related coronavirus 2, isolate USA-WA1/2020, NR-52281 (the Centers for Disease Control and Prevention is the location to deposit the reagent).

REFERENCES

(1) Wang, C.; Horby, P. W.; Hayden, F. G.; Gao, G. F. *Lancet* **2020**, *395*, 470−473.
(2) Huang, C. L.; Wang, Y. M.; Li, X. W.; Ren, L. L.; Zhao, J. P.; Hu, Y.; Zhang, L.; Fan, G. H.; Xu, J. Y.; Gu, X. Y.; Cheng, Z. S.; Yu, T.; Xia, J. A.; Wei, Y.; Wu, W. J.; Xie, X. L.; Yin, W.; Li, H.; Liu, M.; Xiao, Y.; Gao, H.; Guo, L.; Xie, J. G.; Wang, G. F.; Jiang, R. M.; Gao, Z. C.; Jin, Q.; Wang, J. W.; Cao, B. *Lancet* **2020**, *395*, 497−506.
(3) Lalli, M. A.; Langmade, S. J.; Chen, X. H.; Fronick, C. C.; Sawyer, C. S.; Burcea, L. C.; Wilkinson, M. N.; Fulton, R. S.; Heinz, M.; Buchser, W. J.; Head, R. D.; Mitra, R. D.; Milbrandt, J. *Clin. Chem.* **2021**, *67*, 415−424.
(4) Yuan, X.; Yang, C. M.; He, Q.; Chen, J. H.; Yu, D. M.; Li, J.; Zhai, S. Y.; Qin, Z. F.; Du, K.; Chu, Z. H.; Qin, P. W. *Acs. Infect. Dis.* **2020**, *6*, 1998−2016.
(5) Liu, R.; Han, H.; Liu, F.; Lv, Z. H.; Wu, K. L.; Liu, Y. L.; Feng, Y.; Zhu, C. L. *Clin. Chim. Acta* **2020**, *505*, 172−175.
(6) Vandenberg, O.; Martiny, D.; Rochas, O.; van Belkum, A.; Kozlakidis, Z. *Nat. Rev. Microbiol.* **2021**, *19*, 171−183.
(7) Liu, G. Q.; Rusling, J. F. *ACS Sensors* **2021**, *6*, 593−612.
(8) Jin, Z. M.; Du, X. Y.; Xu, Y. C.; Deng, Y. Q.; Liu, M. Q.; Zhao, Y.; Zhang, B.; Li, X. F.; Zhang, L. K.; Peng, C.; Duan, Y. K.; Yu, J.; Wang, L.; Yang, K. L.; Liu, F. J.; Jiang, R. D.; Yang, X. L.; You, T.; Liu, X. C.; Yang, X. N.; Bai, F.; Liu, H.; Liu, X.; Guddat, L. W.; Xu, W. Q.; Xiao, G. F.; Qin, C. F.; Shi, Z. L.; Jiang, H. L.; Rao, Z. H.; Yang, H. T. *Nature* **2020**, *582*, 289−293.
(9) Rut, W.; Lv, Z. Y.; Zmudzinski, M.; Patchett, S.; Nayak, D.; Snipas, S. J.; El Oualid, F.; Huang, T. T.; Bekes, M.; Drag, M.; Olsen, S. K. *Sci. Adv.* **2020**, *6*, eabd4596.
(10) Pillaiyar, T.; Manickam, M.; Namasivayam, V.; Hayashi, Y.; Jung, S. H. *J. Med. Chem.* **2016**, *59*, 6595−6628.
(11) Gossen, J.; Albani, S.; Hanke, A.; Joseph, B. P.; Bergh, C.; Kuzikov, M.; Costanzi, E.; Manelfi, C.; Storici, P.; Gribbon, P.; Beccari, A. R.; Talarico, C.; Spyrakis, F.; Lindahl, E.; Zaliani, A.; Carloni, P.; Wade, R. C.; Musiani, F.; Kokh, D. B.; Rossetti, G. *ACS Pharmacol. Transl. Sci.* **2021**, *4*, 1079−1095.
(12) Zhang, L. L.; Lin, D. Z.; Sun, X. Y. Y.; Curth, U.; Drosten, C.; Sauerhering, L.; Becker, S.; Rox, K.; Hilgenfeld, R. *Science* **2020**, *368*, 409−412.
(13) Mellott, D. M.; Tseng, C. T.; Drelich, A.; Fajtova, P.; Chenna, B. C.; Kostomiris, D. H.; Hsu, J. S.; Zhu, J. Y.; Taylor, Z. W.; Kocurek, K. I.; Tat, V.; Katzfuss, A.; Li, L. F.; Giardini, M. A.; Skinner, D.; Hirata, K.; Yoon, M. C.; Beck, S.; Carlin, A. F.; Clark, A. E.; Beretta, L.; Maneval, D.; Hook, V.; Frueh, F.; Hurst, B. L.; Wang, H.; Raushel, F. M.; O'Donoghue, A. J.; de Siqueira-Neto, J. L.; Meek, T. D.; McKerrow, J. H. *ACS Chem. Biol.* **2021**, *16*, 642−650.
(14) Feng, Y. X.; Liu, G.; La, M.; Liu, L. *Molecules* **2022**, *27*, 615.
(15) Dey-Rao, R.; Smith, G. R.; Timilsina, U.; Falls, Z.; Samudrala, R.; Stavrou, S.; Melendy, T. *Antivir. Res.* **2021**, *195*, 105183.
(16) Cheng, Y.; Borum, R. M.; Clark, A. E.; Jin, Z. C.; Moore, C.; Fajtova, P.; O'Donoghue, A. J.; Carlin, A. F.; Jokerst, J. V. *Angew. Chem., Int. Ed.* **2022**, *61*, e202113617.
(17) Jin, Z. C.; Mantri, Y.; Retout, M.; Cheng, Y.; Zhou, J. J.; Jorns, A.; Fajtova, P.; Yim, W. J.; Moore, C.; Xu, M.; Creyer, M. N.; Borum, R. M.; Zhou, J. C.; Wu, Z. H.; He, T. Y.; Penny, W. F.; O'Donoghue, A. J.; Jokerst, J. V. *Angew. Chem., Int. Ed.* **2022**, *61*, e202112995.
(18) Rut, W.; Groborz, K.; Zhang, L. L.; Sun, X. Y. Y.; Zmudzinski, M.; Pawlik, B.; Wang, X. Y.; Jochmans, D.; Neyts, J.; Mlynarski, W.; Hilgenfeld, R.; Drag, M. *Nat. Chem. Biol.* **2021**, *17*, 222−228.
(19) Garland, G. D.; Harvey, R. F.; Mulroney, T. E.; Monti, M.; Fuller, S.; Haigh, R.; Gerber, P. P.; Barer, M. R.; Matheson, N. J.; Willis, A. E. *Biochem. J.* **2022**, *479*, 901−920.
(20) Jin, Z. C.; Yeung, J.; Zhou, J. J.; Cheng, Y.; Li, Y.; Mantri, Y.; He, T. Y.; Yim, W. J.; Xu, M.; Wu, Z. H.; Fajtova, P.; Creyer, M. N.; Moore, C.; Fu, L.; Penny, W. F.; O'Donoghue, A. J.; Jokerst, J. V. *Chem. Mater.* **2022**, *34*, 1259−1268.
(21) Zhou, J. J.; Creyer, M. N.; Chen, A.; Yim, W.; Lafleur, R. P. M.; He, T. Y.; Lin, Z. X.; Xu, M.; Abbasi, P.; Wu, J. F.; Pascal, T. A.; Caruso, F.; Jokerst, J. V. *J. Am. Chem. Soc.* **2021**, *143*, 12138−12144.
(22) Zhou, J. J.; Xu, M.; Jin, Z. C.; Borum, R. M.; Avakyan, N.; Cheng, Y.; Yim, W.; He, T. Y.; Zhou, J. C.; Wu, Z. H.; Mantri, Y.; Jokerst, J. V. *Angew. Chem., Int. Ed.* **2021**, *60*, 26357−26362.
(23) Yim, W. J.; Takemura, K.; Zhou, J. J.; Zhou, J. C.; Jin, Z. C.; Borum, R. M.; Xu, M.; Cheng, Y.; He, T. Y.; Penny, W.; Miller, B. R.; Jokerst, J. V. *ACS Nano* **2022**, *16*, 683−693.
(24) Xu, M.; Yim, W.; Zhou, J. J.; Zhou, J. C.; Jin, Z. C.; Moore, C.; Borum, R.; Jorns, A.; Jokerst, J. V. *IEEE Nanotechnol. Mag.* **2021**, *15*, 8−28.
(25) Zhou, J. J.; Penna, M.; Lin, Z. X.; Han, Y. Y.; Lafleur, R. P. M.; Qu, Y. J.; Richardson, J. J.; Yarovsky, I.; Jokerst, J. V.; Caruso, F. *Angew. Chem., Int. Ed.* **2021**, *60*, 20225−20230.
(26) He, T. Y.; Bradley, D. G.; Zhou, J. J.; Jorns, A.; Mantri, Y.; Hanna, J. V.; Jokerst, J. V. *ACS Appl. Nano Mater.* **2021**, *4*, 3877−3886.
(27) Jin, Z. C.; Jorns, A.; Yim, W. J.; Wing, R.; Mantri, Y.; Zhou, J. J.; Zhou, J. C.; Wu, Z. H.; Moore, C. H.; Penny, W. F.; Jokerst, J. V. *Anal. Chem.* **2021**, *93*, 11025−11032.
(28) Geethakumari, A. M.; Ahmed, W. S.; Rasool, S.; Fatima, A.; Uddin, S. M. N.; Aouida, M.; Biswas, K. H. A genetically encoded BRET-based SARS-CoV-2 Mpro protease activity sensor. *bioRxiv (Biophysics)*, February 1, 2022, 478460. DOI: 10.1101/2022.01.31.478460.
(29) Mathieu, C.; Touret, F.; Jacquemin, C.; Janin, Y. L.; Nougairede, A.; Brailly, M.; Mazelier, M.; Decimo, D.; Vasseur, V.; Hans, A.; Valle-Casuso, J. C.; de Lamballerie, X.; Horvat, B.; Andre, P.; Si-Tahar, M.; Lotteau, V.; Vidalain, P. O. *Viruses* **2021**, *13*, 1814.
(30) Cheng, H. B.; Li, Y. Y.; Tang, B. Z.; Yoon, J. *Chem. Soc. Rev.* **2020**, *49*, 21−31.
(31) Xu, M.; Kelley, S. P.; Glass, T. E. *Angew. Chem., Int. Ed.* **2018**, *57*, 12741−12744.
(32) Xu, M.; Yin, C. X.; Huo, F. J.; Zhang, Y. B.; Chao, J. B. *Sens. Actuator B Chem.* **2014**, *204*, 18−23.
(33) Kang, J. M.; Li, Z.; Organ, C. L.; Park, C. M.; Yang, C. T.; Pacheco, A.; Wang, D. F.; Lefer, D. J.; Xian, M. *J. Am. Chem. Soc.* **2016**, *138*, 6336−6339.
(34) Wu, Z.; Zhou, J.; Nkanga, C. I.; Jin, Z.; He, T.; Borum, R. M.; Yim, W.; Zhou, J.; Cheng, Y.; Xu, M.; Steinmetz, N. F.; Jokerst, J. V. *ACS Appl. Mater. Interfaces* **2022**, *14*, 13692−13702.
(35) Froggatt, H. M.; Heaton, B. E.; Heaton, N. S. *J. Virol.* **2020**, *94*, e01265-20.
(36) Liew, S. S.; Zeng, Z. L.; Cheng, P. H.; He, S. S.; Zhang, C.; Pu, K. Y. *J. Am. Chem. Soc.* **2021**, *143*, 18827−18831.
(37) Little, T. A. *BiopPharm. Int.* **2015**, *28*, 48−51.

https://doi.org/10.1021/acs.analchem.2c02381
Anal. Chem. 2022, 94, 11728−11733